

# The Influence of Intraseasonal Oscillations on Humid Heat in the Persian Gulf and South Asia

CATHERINE IVANOVICH,<sup>a</sup> WESTON ANDERSON,<sup>b,c</sup> RADLEY HORTON,<sup>d</sup> COLIN RAYMOND,<sup>e</sup> AND ADAM SOBEL<sup>a,d,f</sup>

<sup>a</sup> *Earth and Environmental Sciences, Columbia University, New York, New York*

<sup>b</sup> *International Research Institute for Climate and Society, Palisades, New York*

<sup>c</sup> *Earth System Science Interdisciplinary Center, University of Maryland, College Park, College Park, Maryland*

<sup>d</sup> *Lamont-Doherty Earth Observatory, Columbia University, Palisades, New York*

<sup>e</sup> *Jet Propulsion Laboratory, California Institute of Technology, Pasadena, California*

<sup>f</sup> *Applied Physics and Applied Mathematics, Columbia University, New York, New York*

(Manuscript received 25 June 2021, in final form 10 March 2022)

**ABSTRACT:** Humans' essential ability to combat heat stress through sweat-based evaporative cooling is modulated by ambient air temperature and humidity, making humid heat a critical factor for human health. In this study, we relate the occurrence of extreme humid heat in two focus regions to two related modes of intraseasonal climate variability: the Madden-Julian oscillation (MJO) and the boreal summer intraseasonal oscillation (BSISO). In the Persian Gulf and South Asia during the May–June and July–August seasons, wet-bulb temperatures of 28°C are found to be almost twice as likely during certain oscillation phases than in others. Variations in moisture are found, to varying degrees, to be an important ingredient in anomalously high wet-bulb temperatures in all three areas studied, influenced by distinct local circulation anomalies. In the Persian Gulf, weakening of climatological winds associated with the intraseasonal oscillation's propagating center of convection allows for anomalous onshore advection of humid air. Anomalously high wet-bulb temperatures in the northwestern region of South Asia are closely aligned with positive specific humidity anomalies associated with the convectively active phase of the oscillation. On the southeastern coast of India, high wet-bulb temperatures are associated with convectively inactive phases of the intraseasonal oscillation, suggesting that they may be driven by increased surface insolation and reduced evaporative cooling during monsoon breaks. Our results aid in building a foundation for subseasonal predictions of extreme humid heat in regions where it is highly impactful.

**SIGNIFICANCE STATEMENT:** Understanding when and why extreme humid heat occurs is essential for informing public health efforts protecting against heat stress. This analysis works to improve our understanding of humid heat variability in two at-risk regions, the Persian Gulf and South Asia. By exploring how subseasonal oscillations affect daily extreme events, this analysis helps bridge the prediction gap between weather and climate. We find that extreme humid heat is more than twice as likely during specific phases of these oscillations than in others. Extremes depend to different extents upon combinations of above-average temperature and humidity. This new knowledge of the regional drivers of humid heat variability is important to better prepare for the increasingly widespread health and socioeconomic impacts of heat stress.


**KEYWORDS:** Atmosphere; Subtropics; Madden-Julian oscillation; Climate variability; Humidity; Temperature; Intraseasonal variability; Oscillations


## 1. Introduction

Heat stress is one of the leading causes of death associated with climate extremes (Kovats and Hajat 2008). As such, recent scientific literature has begun to narrow in on the urgency of adapting to extreme humid heat and minimizing

its future progression through the mitigation of greenhouse gas emissions. Recent studies center the influence of humid heat on evaporative cooling and its direct physiological link to human health (Buzan and Huber 2020; Kjellstrom et al. 2016; Sherwood and Huber 2010). At temperatures greater than the human body temperature, evaporative cooling via sweating is the only mechanism through which humans can shed heat (Gagnon and Crandall 2018). However, high air humidity can significantly reduce the efficacy of this essential cooling mechanism. Humid heat thus serves as an important environmental predictor of heat stress.

One metric for measuring humid heat is wet-bulb temperature. Wet-bulb temperature refers to the adiabatic saturation temperature, describing the lowest temperature a parcel of air in contact with liquid water could reach at equilibrium if it were cooled and moistened by evaporation of that water, adiabatically and at constant pressure, to the point of saturation

 Denotes content that is immediately available upon publication as open access.

 Supplemental information related to this paper is available at the Journals Online website: <https://doi.org/10.1175/JCLI-D-21-0488.s1>.

*Corresponding author:* Catherine Ivanovich, cci2107@columbia.edu

DOI: 10.1175/JCLI-D-21-0488.1

© 2022 American Meteorological Society. For information regarding reuse of this content and general copyright information, consult the [AMS Copyright Policy \(www.ametsoc.org/PUBSReuseLicenses\)](#).

(e.g., [Bohren and Albrecht 1998](#)). When the wet-bulb temperature of the air rises above skin temperature at approximately 35°C, humans' evaporative cooling mechanisms can no longer function effectively. Regardless of the health of a person or their access to shade and water, sustained exposure to wet-bulb temperatures above this threshold will inevitably lead to heat illness and death ([Parsons 2006](#)). Detrimental health impacts can also occur far below this threshold, particularly for outdoor laborers and those with preexisting health conditions ([Vecellio et al. 2022](#); [Zander et al. 2015](#); [Borg et al. 2021](#); [Leon and Bouchama 2015](#); [Semenza et al. 1999](#)). In comparison to other metrics used to quantify humid heat and heat stress, wet-bulb temperature is unique in its ability to provide a clearly defined threshold above which humans cannot sustain healthy body temperatures without the help of artificial cooling ([Sherwood and Huber 2010](#); [Buzan et al. 2015](#)).

Humid heat exposure is expected to rise dramatically over the twenty-first century. Exposure to extreme wet-bulb temperatures is projected to increase most in the tropics and subtropics, large portions of which currently lack sufficient infrastructure and resources to supply artificial cooling to all inhabitants, and which are projected to experience a simultaneous increase in population ([Coffel et al. 2018](#)). By 2080, more than a million person-days of intolerable levels of extreme humid heat could be observed under the high emissions scenario representative concentration pathway 8.5 (RCP8.5) ([Coffel et al. 2018](#)), and under less aggressive warming scenarios these impacts may be observed in following decades. While a large amount of research has been dedicated to the occurrence of extreme dry heat ([Raymond et al. 2019](#); [Horton et al. 2016](#)), the projected increases in the exposure to heat stress have generally been found to depend more on local increases in specific humidity than on local increases in temperature ([Lutsko 2020](#)).

Two regions that have already experienced intolerable levels of humid heat in recent years are the Persian Gulf basin and South Asia ([Raymond et al. 2020](#)). Throughout the summer season, strong northwesterly surface "shamal" winds bring hot and dry air from Mesopotamia over the Persian Gulf ([Nasrallah et al. 2004](#)). Widespread subsidence occurs during the summer, raising temperatures by encouraging clear sky conditions. By allowing high absorption of solar radiation, clear skies raise temperatures both over land and over the adjacent shallow, low-albedo Persian Gulf and Red Sea, where sea surface temperatures can rise well above 30°C ([Rodwell and Hoskins 1996](#); [Raymond et al. 2020](#)). The even higher air temperatures over the water encourage increased evaporation rates, meaning that high humid heat conditions can occur on land with just a weak sea breeze ([Raymond et al. 2021](#); [Pal and Eltahir 2016](#); [Xue and Eltahir 2015](#)). While the boundary layer can remain humid over the ocean and coastal regions, subsidence suppresses convection (and the associated ventilation of the boundary layer) by drying the free troposphere ([Prasanna and Annamalai 2012](#)). Major cities around the Persian Gulf are projected to experience large increases in the frequency and magnitude of dangerous wet-bulb temperatures over the twenty-first century, particularly daunting for outdoor laborers who are already exposed to dangerous

levels of humid heat in countries such as Qatar ([Pal and Eltahir 2016](#); [Pradhan et al. 2019](#)).

In South Asia, humid heat is strongly affected by the South Asian summer monsoon, which advects warm and humid air from the Arabian Sea and Bay of Bengal into inland areas ([Monteiro and Caballero 2019](#); [Acosta and Huber 2017](#)). Humid heat in South Asia is further exacerbated by human activity, where widespread irrigation tends to increase humidity over much of the region ([Im et al. 2014](#); [Mishra et al. 2020](#); [Kraukauer et al. 2020](#)). Extreme humid heat has been projected to increase significantly in South Asia over the twenty-first century, where a once-per-25-yr wet-bulb temperature extreme event in today's climate may become a yearly occurrence by the end of the century under the aggressive RCP8.5 warming scenario ([Im et al. 2017](#)).

While recent literature has begun to explore specific conditions associated with the occurrence of extreme humid heat in regions such as the Persian Gulf and South Asia, research has not yet examined the modulation of local wet-bulb temperatures by large-scale modes of climate variability. One such example is intraseasonal oscillations such as the Madden-Julian oscillation (MJO) and the related boreal summer intraseasonal oscillation (BSISO) ([Jiang et al. 2020](#)). The MJO describes a coupled pattern of large-scale circulation and convection in the tropics that propagates eastward with a period of roughly 30–60 days. The BSISO can be considered the summer counterpart to the MJO that exhibits more complex northward or northeastward propagation and whose centers of convection reach latitudes well north of the equator ([Yasunari 1979](#); [Sikka and Gadgil 1980](#); [Jiang et al. 2004](#); [Adames et al. 2016](#); [Lawrence and Webster 2002](#)). The location and period of these oscillations render them the dominant modes of subseasonal variability in the tropics. The influence of intraseasonal oscillations, however, reaches well beyond the tropics via atmospheric teleconnections to variables such as temperature and precipitation in regions as diverse as North America ([Arcodia et al. 2020](#); [Zhou et al. 2012](#); [Lin and Brunet 2009](#)), South America ([Alvarez et al. 2016](#)), Australia ([Wheeler et al. 2008](#)), southwest Asia ([Barlow et al. 2005](#)), South Asia ([Joseph et al. 2009](#)), and East Asia ([Jeong et al. 2005](#)). The widespread influence of intraseasonal oscillations on global climate makes them potentially important sources of joint heat–humidity variability. Forecasts of the MJO and BSISO have improved in recent years, with predictive skill increasing to about four weeks ([Jiang et al. 2020](#); [Vitart 2017](#)). Leveraging this skill could allow for better prediction and preparation for the impacts of heat stress, especially in regions that already experience dangerous levels of humid heat such as the Persian Gulf and South Asia ([Coughlan de Perez et al. 2018](#)).

In this study, we investigate the variability of humid heat on a subseasonal-to-seasonal time scale by examining the influence of intraseasonal oscillations on both extreme and mean wet-bulb temperatures in the Persian Gulf and South Asia. [Section 2](#) outlines the data sources and methodology for generating wet-bulb temperature composites. The results of these composite analyses are presented and compared in [section 3](#). [Section 4](#) provides a discussion of the potential

physical mechanisms that lead to the identified patterns in wet-bulb temperature extremes and anomalies. Finally, a summary of the main conclusions and directions for future research are presented in [section 5](#).

## 2. Methods

### a. Data sources

The analysis presented in this study uses both station-based and reanalysis datasets. Quality-controlled station data from the Met Office Hadley Centre Integrated Surface Database (HadISD) dataset includes subdaily measurements of variables such as surface temperature, pressure, and dewpoint temperature for a total of 7877 stations around the world ([Dunn 2019](#)). While the temporal resolution of this dataset varies for each station location, the resolution tends to increase with time; many stations provide hourly data coverage in the most recent years of data collection. All stations were screened for data reliability based on a stringent set of checks as detailed in [Raymond et al. \(2020\)](#). Selecting for stations that only pass these criteria reduces the global station count to 4576, the number used throughout our analysis.

Data from the fifth major global reanalysis produced by the European Centre for Medium-Range Weather Forecasts (ERA5) high-resolution product including 2-m air temperature, 2-m dewpoint temperature, outgoing longwave radiation (OLR), surface pressure, and 10-m winds were also used to analyze potential physical mechanisms influencing the modulation of wet-bulb temperature by the MJO and BSISO ([Hersbach et al. 2020](#)). ERA5 provides hourly data with a 30 km spatial resolution. Each of the retrieved variables are then converted to daily mean values at each grid point.

To determine the phase and amplitude of the intraseasonal oscillations, the all-season OLR-based MJO index (OMI) was selected ([Kiladis et al. 2014](#)). The OMI is based on empirical orthogonal function (EOF) analyses of ERA-Interim OLR centered on the equator between 20°S and 20°N. This index has an improved ability to capture the wide spectrum of disturbances taking place in the June–August season in comparison to traditional indices such as the real-time multivariate MJO (RMM) index, while also being applicable to other months ([Wang et al. 2018](#); [Wheeler and Hendon 2004](#)). This index thus helps to capture the signal of the BSISO in addition to the MJO, while better reproducing the signal's northward propagation. These unique aspects of the OMI are particularly important to the analysis here, as wet-bulb temperatures can reach extreme values in the Persian Gulf and South Asia during the months May–August and both regions are well north of the equator. The BSISO tends to dominate the subseasonal-to-seasonal variability signal in the northern Indian Ocean during the months June–August ([Wang et al. 2018](#); [Wang and Xie 1997](#)). However, the distinction between MJO and BSISO events is somewhat subjective and variable within the literature, and the two modes are arguably seasonally varying manifestations of the same underlying dynamics ([Wang and Sobel 2022](#)). Thus, we do not draw a distinction, and consider the patterns identified in this analysis to be

associated with phases describing the propagation of both the BSISO and MJO. To allow for comparison to recent literature, analyses were also reproduced using the RMM index with few qualitative differences in resulting phase patterns (Fig. S1 in the online supplemental material). Time series of both indices were accessed directly from the respective authors' published datasets ([Kiladis et al. 2014](#); [Wheeler and Hendon 2004](#)).

Wet-bulb temperature is calculated from surface temperature, pressure, and dewpoint temperature through the Davies-Jones method ([Davies-Jones 2008](#)). The Davies-Jones method involves an iterative algorithm using Bolton's formula for equivalent potential temperature, through which the wet-bulb temperature on a specific pseudoadiabatic and pressure surface can be generated. This method is preferred over others such as the Stull method ([Stull 2011](#)) due to its increased accuracy from taking pressure dependence into account ([Buzan et al. 2015](#)). The difference between wet-bulb temperatures calculated using these contrasting methods are pronounced at high values, with the Stull method underestimating true wet-bulb temperatures by over 1°C. The daily maximum wet-bulb temperature was retained from the HadISD datasets, along with the co-occurring temperature and specific humidity values. The daily mean wet-bulb temperature was calculated from the ERA5 datasets in order to analyze the influence of intraseasonal oscillations on mean humid heat conditions in each region. While daily maximum wet-bulb temperatures can determine whether extreme thresholds dangerous to human health have been exceeded, daily mean values are also important, as they can better reflect nighttime wet-bulb temperatures, which have been strongly linked to heat stress ([Buzan and Huber 2020](#); [Di Napoli et al. 2019](#)). Previous literature has demonstrated that reanalysis products systematically underestimate extreme wet-bulb temperatures in high-risk regions such as the Persian Gulf and South Asia (e.g., [Raymond et al. 2020](#)). However, the magnitude of mean wet-bulb temperature anomalies identified throughout this analysis are generally in strong agreement between both the HadISD and ERA5 datasets.

### b. Composites

Seasonal composites of daily maximum wet-bulb temperature were generated using the HadISD station data for three regions of interest: the Persian Gulf (20°–36°N, 45°–60°E), northwestern South Asia (22°–32°N, 68°–78°E), and southeastern India (8°–22°N, 78°–90°E). The two subregions of South Asia were defined by considering areas that experience the greatest levels of extreme humid heat and dividing them based on the climatological onset date of the summer monsoon, which is typically more than a month later in northwestern South Asia than in southeastern India ([Qian and Lee 1999](#)). The presented results are broken down into 2-month seasons, namely, May–June (MJ) and July–August (JA). Throughout this analysis, a wet-bulb temperature of 28°C was selected as an extreme threshold as it retains a sufficiently large number of data points while still being associated with major human health impacts ([Cheng et al. 2019](#); [Mora et al.](#)

2017). The relative difference in extreme humid heat frequency between the three subregions becomes more apparent at higher absolute thresholds, but the sample size becomes too limited to generate statistically significant patterns. Regional composites are generated using data from the 2-month season that climatologically exhibit the highest number of daily maximum wet-bulb temperatures over 28°C (Fig. S2), herein referred to as the “humid heat season”; this corresponds to MJ for southeastern India and JA for both the Persian Gulf and northwestern South Asia. We note that stations in India that are not included in the two subregions of South Asia almost never surpass the 28°C wet-bulb temperature threshold, a previously observed spatial pattern (Raymond et al. 2020; Monteiro and Caballero 2019; Im et al. 2017).

The likelihood of surpassing an extreme wet-bulb temperature threshold of 28°C during each phase of the oscillation was evaluated for each region. The results presented here center on the single station in each region that has experienced the highest number of wet-bulb temperature events above 28°C in the region’s respective humid heat season. These extreme wet-bulb temperature exceedance frequencies are conditioned by the number of days observed in each oscillation phase (i.e., given the oscillation is in a specific phase, how likely is the daily maximum wet-bulb temperature to exceed the 28°C threshold). For concision, we define the “peak extreme phase” as the phase when the highest likelihood of exceeding various wet-bulb temperature extremes are identified and the “peak anomaly phase” as the phase with the highest average wet-bulb temperature anomaly. These values are compared to the overall (phase independent) likelihood of exceeding the threshold. To determine the significance of this comparison, we conducted a Monte Carlo resampling in which the oscillation phase associated with the time series for each station was randomized without replacement 500 times. The likelihood of surpassing 28°C for each phase of the oscillation in each season was computed for every randomization, and the 95th and 5th percentiles were computed. We verified that the patterns identified for each of the three stations of interest are qualitatively consistent for higher absolute wet-bulb temperature thresholds (30° and 32°C) (Figs. S3 and S4). A mirrored analysis conducted by averaging the likelihood of surpassing a 28°C threshold over all stations in each region can be found in Fig. S5.

To evaluate potential physical mechanisms influencing the relationship between the intraseasonal oscillations and humid heat, composites of the ERA5 data were also generated for daily average anomalies of wet-bulb temperature, dry-bulb temperature, and specific humidity alongside the mean climatology of these variables in each region. These composites also include the mean OLR and surface wind anomalies associated with each phase of the oscillation in order to track the location of the center of convection and the potential influence of temperature and moisture advection. The statistical significance of patterns identified in these composite maps is evaluated using a two-step testing method. We first perform a Student’s *t* test to determine whether the patterns in each phase are statistically different from those in phase 0 (the inactive phase of the MJO and BSISO) to 95% confidence.

We then employ the methodology described by Wilks (2016) to test for field significance, evaluating whether an equal number of significant findings in each phase can be expected by chance alone.

### 3. Results

#### a. Local station-based composites

Figure 1 plots HadISD station locations colored by the oscillation phase during which they experience the highest average daily maximum wet-bulb temperature in the MJ and JA seasons. A regional coherence emerges: clear northward-tilting bands of locations experience their maximum daily wet-bulb temperature in the same oscillation phase, and these bands move northeastward with increasing phase (noting the cyclic nature of the phase index, where the oscillation returns to phase 1 after phase 8). For example, during the JA season, the highest mean daily maximum wet-bulb temperature is experienced in phase 7 for regions such as southwestern India and the Maritime Continent. To the north in central India and Southeast Asia, the highest values are observed in phases 2 and 3. This northward propagation is not strictly monotonic, however, but reverses throughout southeastern China in phases 1 and 6. While the phases with highest average daily maximum wet-bulb temperature at each station are often slightly different when comparing the MJ and JA patterns (e.g., phase 1 throughout the western Persian Gulf in MJ vs phase 3 in JA), these coherent regional bands are visible in both seasons. Figure 1 thus suggests that the MJO and BSISO do present a coherent signal in the wet-bulb temperatures observed in this region during May–August.

At high-risk stations of interest—we analyze Doha, Qatar (Persian Gulf); Jacobabad, Pakistan (northwestern South Asia); and Bhubaneswar, India (southeastern India)—wet-bulb temperatures are almost twice as likely to exceed 28°C in some phases as in others (Fig. 2). In the JA season, Doha, Qatar is about 10% more likely to exceed this threshold during phase 3 than the inactive phase of the oscillation, while during phase 8, exceedances are about 20% less likely. A plurality of these extreme wet-bulb temperatures take place in the month of August, consistent with previous literature (Raymond et al. 2020). Although robust over the observational record, these results are complicated by the seasonality of the MJO and BSISO, which tend to spend more days in phases such as 1 and 2 during the July–August season than in other months (Fig. S6). This seasonal dependence is a consequence of the empirical nature of the phase indices used to describe MJO and BSISO propagation (Alvarez et al. 2016; Wheeler et al. 2008), which makes further exploration of definition sensitivity beyond the scope of this work. We also recognize that the distribution of days exceeding the 28°C threshold at each station across each phase may shift with time due to long-term global warming. For example, in the Persian Gulf the annual frequency of exceeding a 28°C threshold has increased the most in phase 2 (0.14 days yr<sup>-1</sup>) and has decreased the most in phase 4 (−0.02 days yr<sup>-1</sup>) over the past 40 years. However, we find that the difference in trends of the



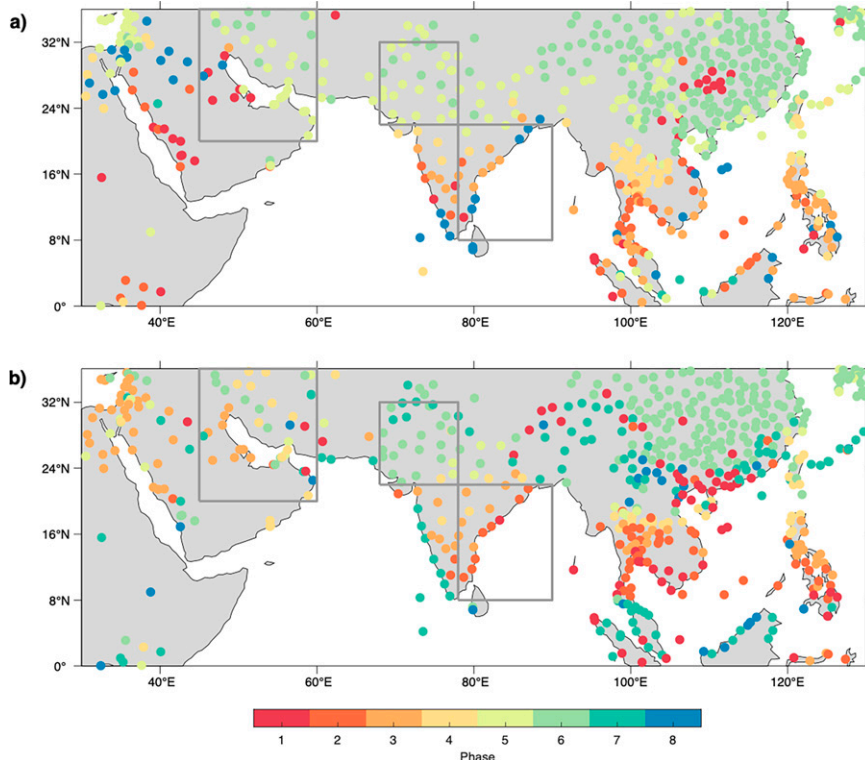


FIG. 1. Regional section of HadISD station map colored by the phase with the highest average daily maximum wet-bulb temperature in (a) May–June and (b) July–August. Gray boxes indicate the locations of three subregions selected for regional analyses; from west to east: Persian Gulf, northwestern South Asia, and southeastern India.

number of days exceeding  $28^{\circ}\text{C}$  each year between oscillation phases is much lower than the year to year variability within each phase, indicating that this aspect of the analysis does not greatly affect the results (Fig. S7–S9).

The two stations analyzed in South Asia are also significantly more likely to surpass  $28^{\circ}\text{C}$  in wet-bulb temperature in certain phases. In Jacobabad, Pakistan, threshold exceedances during phase 6 are the most likely (about 8% more) and least likely in phase 4 (about 15% less). These extreme humid heat exceedances occur primarily during the month of July (Fig. S2), broadly agreeing with previous analyses of Pakistani weather stations (Monteiro and Caballero 2019). There is also a significant difference in the likelihood of  $28^{\circ}\text{C}$  events between oscillation phases in Bhubaneswar, India. Specifically, this likelihood is highest in phases 1 and 8 (about 10% more), and lowest in phase 5 (about 10% less). In southeastern India, wet-bulb temperatures of  $28^{\circ}\text{C}$  or above most often occur in May, prior to the climatological onset of the summer monsoon. More extreme wet-bulb temperatures at thresholds above  $30^{\circ}\text{C}$  are rarely observed in southeastern India during this season (Figs. S4 and S5). There is a slight difference in the identified peak extreme phase and peak anomaly phase at Bhubaneswar (phase 1 vs phase 3). This shift may be associated with the variance of wet-bulb temperatures in each phase, indicating that phase patterns in mean wet-bulb temperature anomalies may not align with those in the

likelihood of extreme events. For example, the increased likelihood of extreme events in phase 1 relative to phase 5 in Bhubaneswar is actually associated with a decrease in the mean wet-bulb temperature in this phase (Fig. S13). Further, because a large number of days in any phase are near the  $28^{\circ}\text{C}$  threshold at this station, small differences in mean wet-bulb temperature from one phase to another can be associated with large differences in the number of extreme threshold crossings, even in the absence of differences in the distributions.

Co-occurring dry-bulb temperature and specific humidity values for daily maximum wet-bulb temperatures experienced by the three analyzed stations in their respective humid heat season are plotted in Fig. 3, based on Raymond et al. (2017). Comparing the relative position of the lowest 50% and highest 10% of wet-bulb temperature events in this bivariate space for each phase composite provides an estimation of the humidity and temperature dependence of its extreme humid heat events, relative to the climatological dependence. The larger (smaller) the vector angle between the horizontal axis and the line connecting squares of the same color in Fig. 3, the greater (lesser) the contribution of anomalous humidity to extremes in a given phase, termed here “humidity dependence” (“temperature dependence”). The orientation of the gray squares in each plot indicates the relative temperature and humidity dependence of extremes at each station across

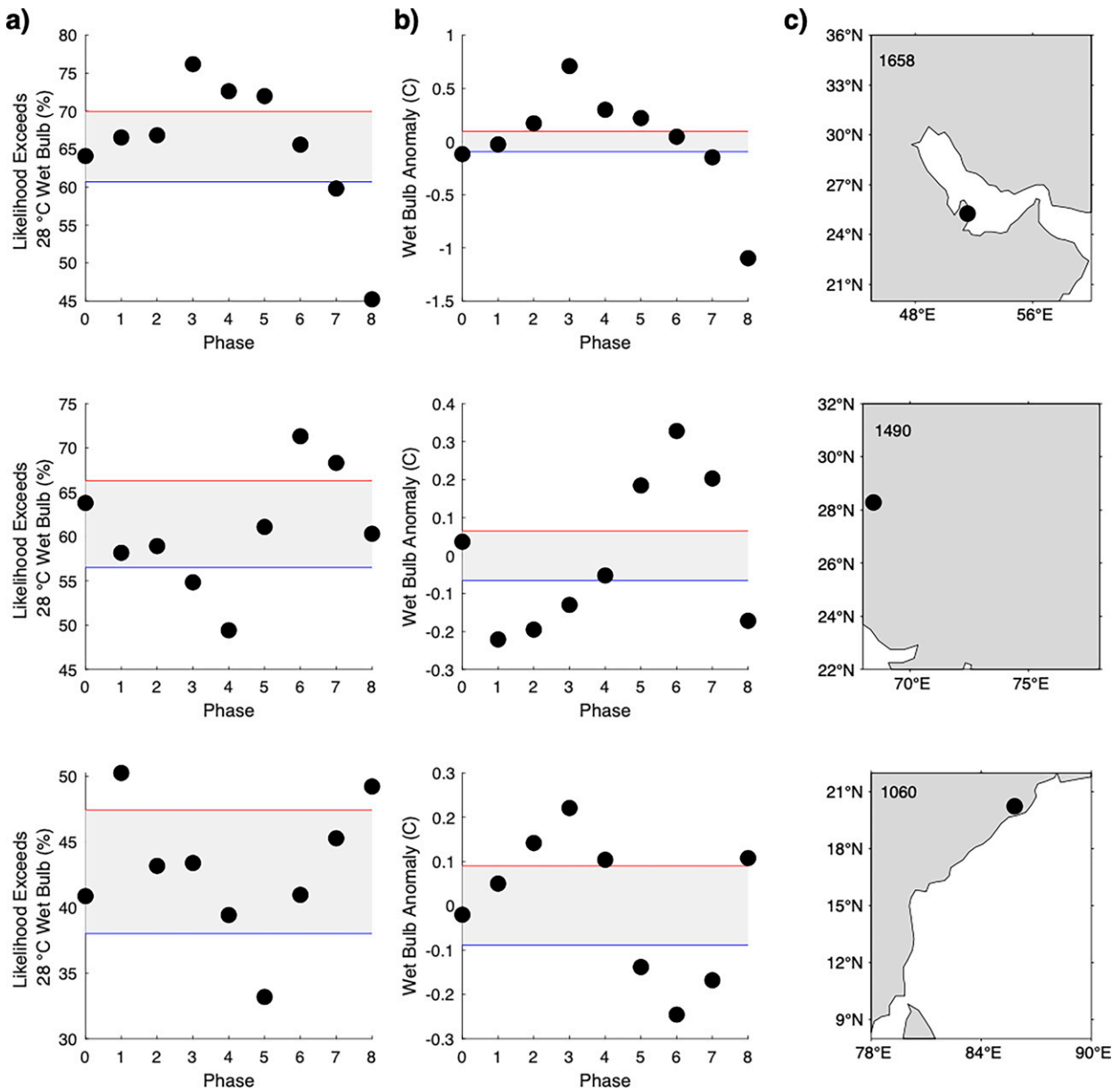


FIG. 2. HadISD station composites for the single station in each region that experiences the greatest total number of extreme wet-bulb temperatures. (a) Likelihood of exceeding 28°C wet-bulb temperature given the oscillation is in each phase. Composites are computed during the 2-month season that observes the highest number of exceedances. These seasons are (top) July–August for Doha, (middle) July–August for Jacobabad, and (bottom) May–June for Bhubaneswar. Red and blue lines indicate upper and lower bounds of 95% confidence intervals (shaded), respectively. Phase 0 indicates neutral phase of intraseasonal oscillations. (b) Mean wet-bulb temperature anomalies associated with each phase during respective humid heat season. (c) Locations of selected stations. The number in the upper-left corner of (c) indicates the number of times the station exceeds 28°C during its respective humid heat season in the station data record.

all days within the season, while the blue squares characterize the shift in this dependence associated with oscillation phase. Figures for each station presenting data for all eight phases of the oscillation are provided in the online supplemental material (Figs. S10–S12).

We next consider differences in humid heat climatology at each station, before progressing to evaluation of their

modulation by subseasonal oscillations. Doha exhibits the largest range in specific humidity over its humid heat season. This is consistent with expectations of the surrounding regional

Persian Gulf climate, which is typically very dry throughout the summer, in combination with the moisture availability afforded by the station due to its coastal location when

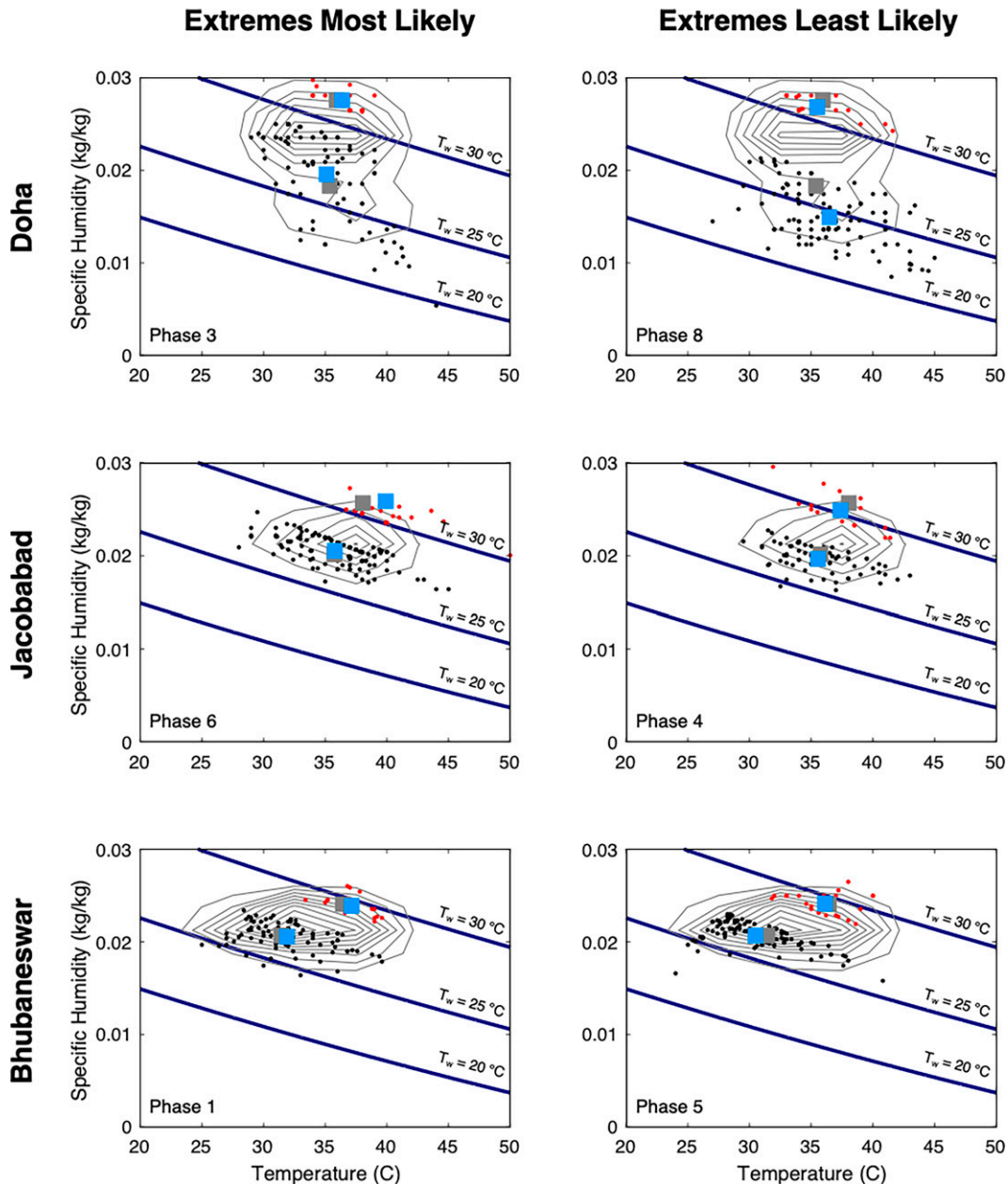


FIG. 3. Temperature and specific humidity occurring at the hour of daily maximum wet-bulb temperature for (top) Doha, (middle) Jacobabad, and (bottom) Bhubaneswar during their respective humid heat season. Phase is indicated in the lower-left corner of each subplot. Red (black) points represent top 10% (lower 50%) of wet-bulb temperatures in the time series. Blue squares are the averages of each percentile grouping within the phase of analysis; gray squares are the average across all phases. Angular orientation between squares of the same color reflects the relative contribution of specific humidity and temperature excursions toward extreme wet-bulb temperatures in a given phase (blue), in comparison to that associated with average conditions in each percentile group across all phases (gray). Gray contours indicate two-dimensional point density for aggregate time series without differentiating between phase (largest contour contains at least 90% of the data series in each region). Heavy blue diagonal lines indicate constant wet-bulb temperatures.

meteorological conditions are favorable (Al Senafi and Anis 2015; Xue and Eltahir 2015). Bhubaneswar exhibits the largest range in temperature, consistent with the fact that the MJ season spans the climatological onset of the summer

monsoon, which is significantly more active in southeastern India than the northwestern part of the region encompassing Jacobabad during these months. Humidity may not vary as greatly as temperature in Bhubaneswar due to the abundant

moisture availability throughout this season. Once the monsoon has commenced, frequent and heavy (but spatially heterogeneous) precipitation is associated with cooling of the surface and near-surface temperatures in Bhubaneswar through evaporative cooling and increased cloud cover. Overall, the almost vertical orientation between the lower 50% and top 10% of daily maximum wet-bulb temperatures in the first row of Fig. 3 (gray squares) indicates that extreme humid heat conditions regardless of oscillation phase are relatively humidity dependent in Doha. In contrast, the greatly flattened orientation between percentile groups in Bhubaneswar reflects relatively temperature dependent extreme humid heat. The relative temperature and humidity dependence of extreme humid heat events in Jacobabad lies in the middle of these two ends of the spectrum.

Compared to these mean conditions for humid heat, we find that anomalously high wet-bulb temperatures in all three stations are relatively more temperature dependent during their respective peak extreme phase. However, these oscillation-associated shifts in the temperature and humidity dependence of extreme events are subtle in comparison to the relative differences between stations. In phase 3, the peak extreme phase in Doha, the most extreme humid heat events depend slightly more on anomalous temperature than during other phases. However, the lowest 50% of wet-bulb temperature days in this phase are also anomalously high and often cross the 28°C threshold, primarily due to increased moisture. In contrast, during phase 8, when the likelihood of exceeding 28°C wet-bulb temperatures is relatively low, the orientation between the humid heat events' top and bottom percentile groups flip and are more humidity dependent than those experienced by the station on average. Moisture appears to be abnormally limited during the bottom 50% of wet-bulb temperature events in phase 8 (Fig. 3), which may explain the reduced frequency of extreme wet-bulb temperatures during this phase (Fig. 2). Thus, in both phase 3 and phase 8, the likelihood of surpassing extreme wet-bulb temperature thresholds is highly influenced by local moisture availability.

Jacobabad also exhibits higher temperature dependence than average during its peak extreme phase, phase 6. While the temperatures and humidities associated with the bottom 50% of wet-bulb temperature events remain rather constant from one phase to another, anomalously high temperatures associated with the top 10% of wet-bulb events during phase 6 facilitate the exceedance of extreme thresholds.

The relative temperature and humidity dependence of wet-bulb extremes in Bhubaneswar is highly consistent from one phase to another (Figs. 3 and S12). During phase 1, the entire distribution is shifted roughly equally toward higher temperatures, triggering an associated increased likelihood for exceeding extreme humid heat thresholds. The opposite is true for phase 5, when anomalously low temperatures are observed in both percentile groups alongside a simultaneous decreased likelihood for wet-bulb temperatures over 28°C.

### *b. Regional reanalysis-based composites*

To investigate the physical mechanisms influencing humid heat in each region on a larger spatial scale, composites of the

ERA5 data are presented in Figs. 4–11 for outgoing longwave radiation, wet-bulb temperature, dry-bulb temperature, and specific humidity. These results build upon the patterns identified in extreme frequency in Fig. 2, as even small shifts in mean humid heat conditions can result in dramatic increases in the likelihood of exceeding extreme wet-bulb temperature thresholds (Fig. S13). In contrast to the at-risk station locations, moisture anomalies dominate mean wet-bulb temperature anomalies across most of the area in the three regions of interest. In phase 3, the peak anomaly phase for both the Persian Gulf reanalysis and Doha station composites (Fig. 7; Fig. 2b), there are clear reductions in the climatological northwesterly shamal winds, which may indicate that easterly sea breezes are able to advect moisture onto the western shore (Raymond et al. 2021). Strong positive specific humidity anomalies and slightly negative temperature anomalies are simultaneously observed during phase 3 in the July–August season (Figs. 9 and 11), indicating that temperature anomalies do not contribute strongly to the elevated wet-bulb temperatures during these phases. OLR anomalies are slightly positive throughout the Persian Gulf in phase 3, then shift to negative in phase 5 (Fig. 5). This transition from suppressed to enhanced convection suggests that atmospheric water vapor may build up while surface temperatures remain high one to two phases before the onset of anomalous precipitation or reduced subsidence associated with the oscillation-driven center of convection. This interpretation is consistent with Feng et al. (2020) who have highlighted the increase in temperature and humidity observed prior to MJO convection onset. In contrast, during phase 8 when there is a relatively low probability of experiencing extreme wet-bulb temperatures in Doha, strong northwesterly surface wind anomalies drive negative temperature and specific humidity anomalies.

In northwestern South Asia, the peak anomaly phase is identified as phase 6 in the July–August season (Fig. 7), agreeing with the station data for Jacobabad (Fig. 2b). During this phase, the spatial pattern in composited wet-bulb temperature anomalies aligns very closely with that of the specific humidity anomaly composites. It is also during phases 5 through 7 that the center of enhanced convection associated with the oscillation moves to the north and passes over the Indian subcontinent (Fig. 4). There are weak temperature anomalies in this region during these phases, where slightly positive anomalies are observed outside the bounds of enhanced convection while slightly negative anomalies occur within. In phases 3 and 4 when both the reanalysis and station composites identify relatively low wet-bulb temperatures, this region experiences high temperature anomalies and strong negative specific humidity anomalies (Figs. 9 and 11). The reanalysis composites are consistent with findings from recent literature that suggest that wet-bulb temperature extremes throughout Pakistan are dependent upon moisture anomalies (Raymond et al. 2020; Monteiro and Caballero 2019). This contrasts with the more temperature-dependent humid heat extremes identified in phase 6 for Jacobabad in Fig. 3, indicating that mechanisms controlling highly localized extreme events may be different from those influencing mean humid heat conditions in the larger surrounding region. This is relatively easy to imagine in a region with such complex topography,



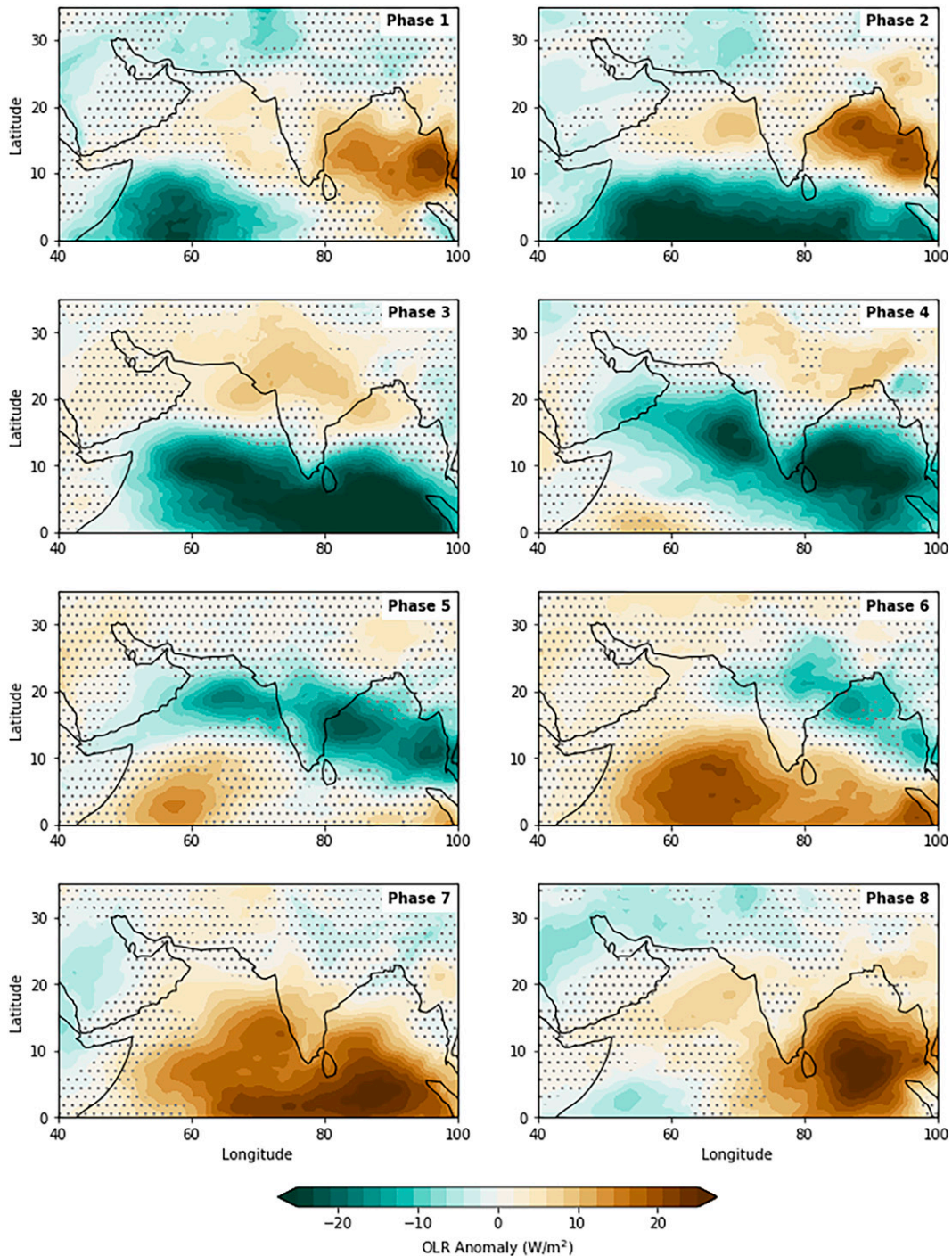


FIG. 4. Composites of daily average outgoing longwave radiation anomalies for May–June during 1979–2019. Negative OLR anomalies indicate increased cloud cover, associated with convection and precipitation. Stippling represents statistically insignificant patterns at a 95% threshold.

heterogeneous lower boundary conditions, and relatively few observations to constrain reanalyses. Further, our results identify strong offshore winds associated with humid heat extremes in this region, opposite to the onshore advection of

humid marine air previously identified as central to extreme humid heat events in Pakistan by [Monteiro and Caballero \(2019\)](#). This difference may indicate that the anomalous humidity associated with the oscillation center of convection

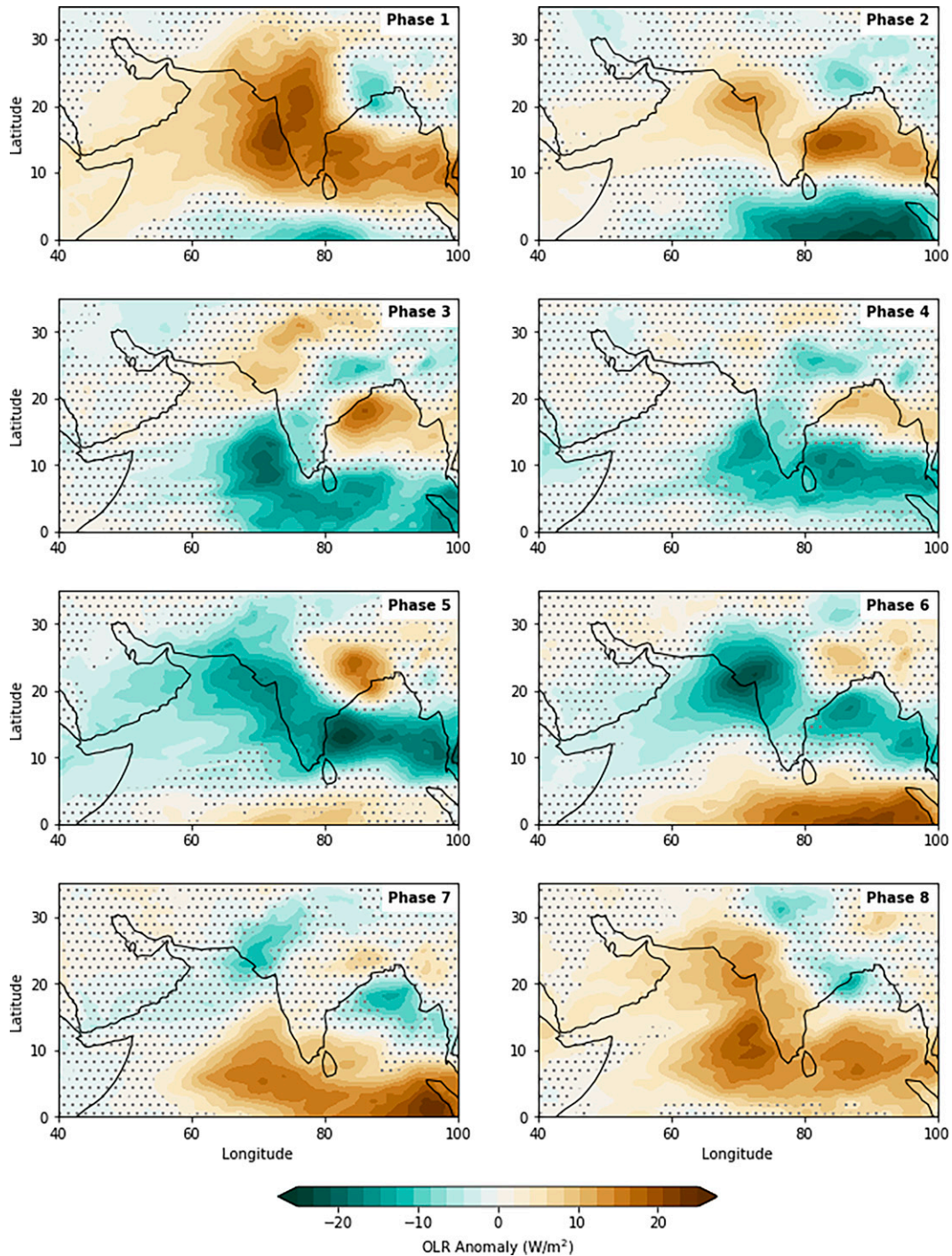


FIG. 5. Composites of daily average outgoing longwave radiation anomalies for July–August during 1979–2019. Negative OLR anomalies indicate increased cloud cover, associated with convection and precipitation. Stippling represents statistically insignificant patterns at a 95% threshold.

dominates the humid heat conditions in this region during this phase compared to these typical advective mechanisms.

Circulation anomalies incident with the MJO and BSISO may be associated with monsoon breaks in southeastern India during the May–June season (Joseph et al. 2009), leading to

elevated wet-bulb temperatures. The peak anomaly phase in the reanalysis composites for the humid heat season in this region is phase 3 (Fig. 6), consistent with station composites of the same metric (Fig. 2b). During this phase, there are strong positive specific humidity and temperature anomalies



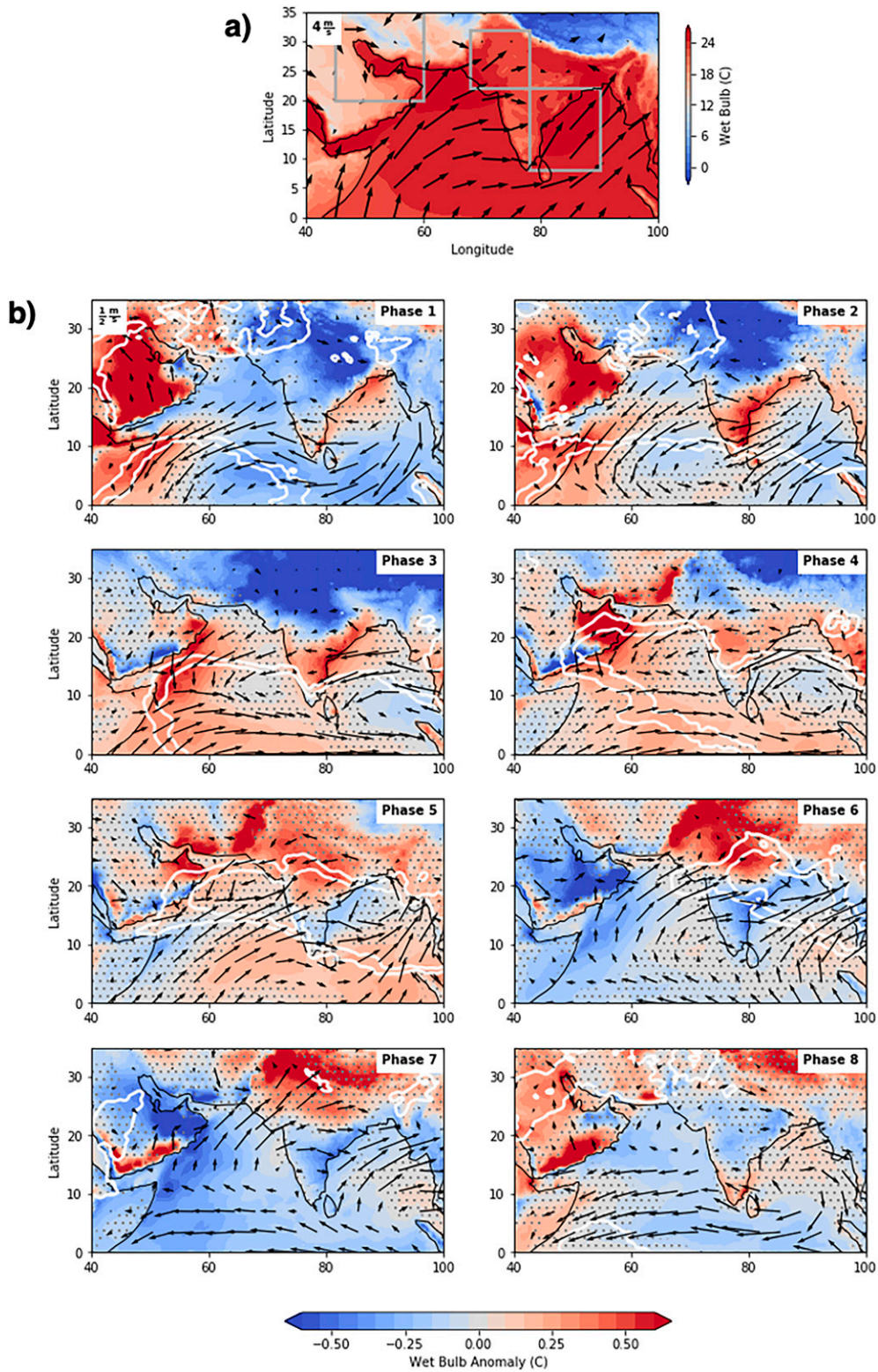


FIG. 6. ERA5 composites of daily mean 2-m wet-bulb temperature for May–June. (a) Climatology of the region and (b) composites of daily anomalies by oscillation phase. White contours indicate location of oscillation phase defined by OLR anomalies less than  $-4 \text{ W m}^{-2}$ , and vectors indicate surface wind anomalies. Stippling represents statistically insignificant patterns at a 95% threshold.

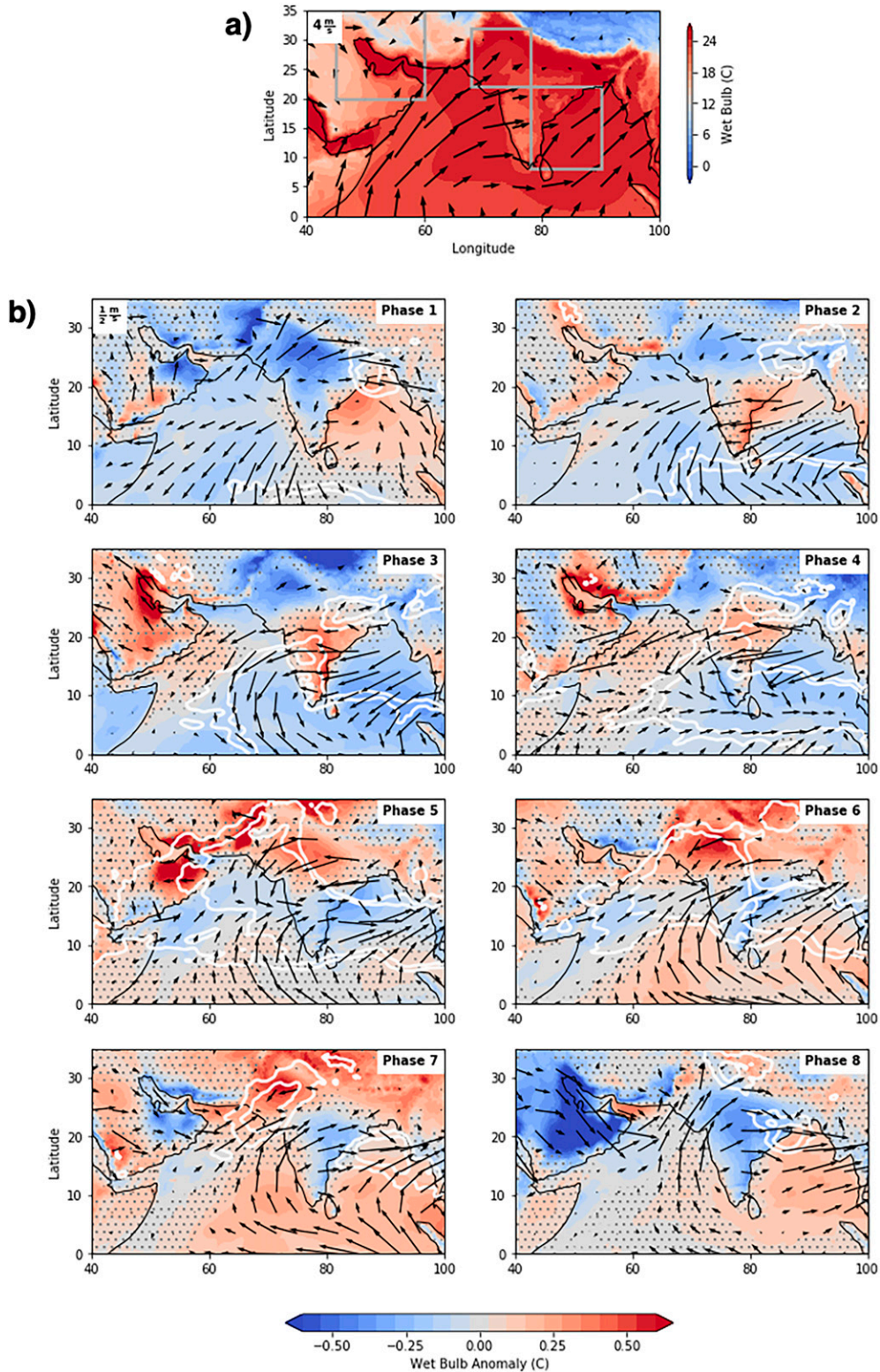


FIG. 7. ERA5 composites of daily mean 2-m wet-bulb temperature for July–August. (a) Climatology of the region and (b) composites of daily anomalies by oscillation phase. White contours indicate location of oscillation phase. White contours indicate location of oscillation-related convection defined by OLR anomalies less than  $-4 \text{ W m}^{-2}$ , and vectors indicate surface wind anomalies. Stippling represents statistically insignificant patterns at a 95% threshold.



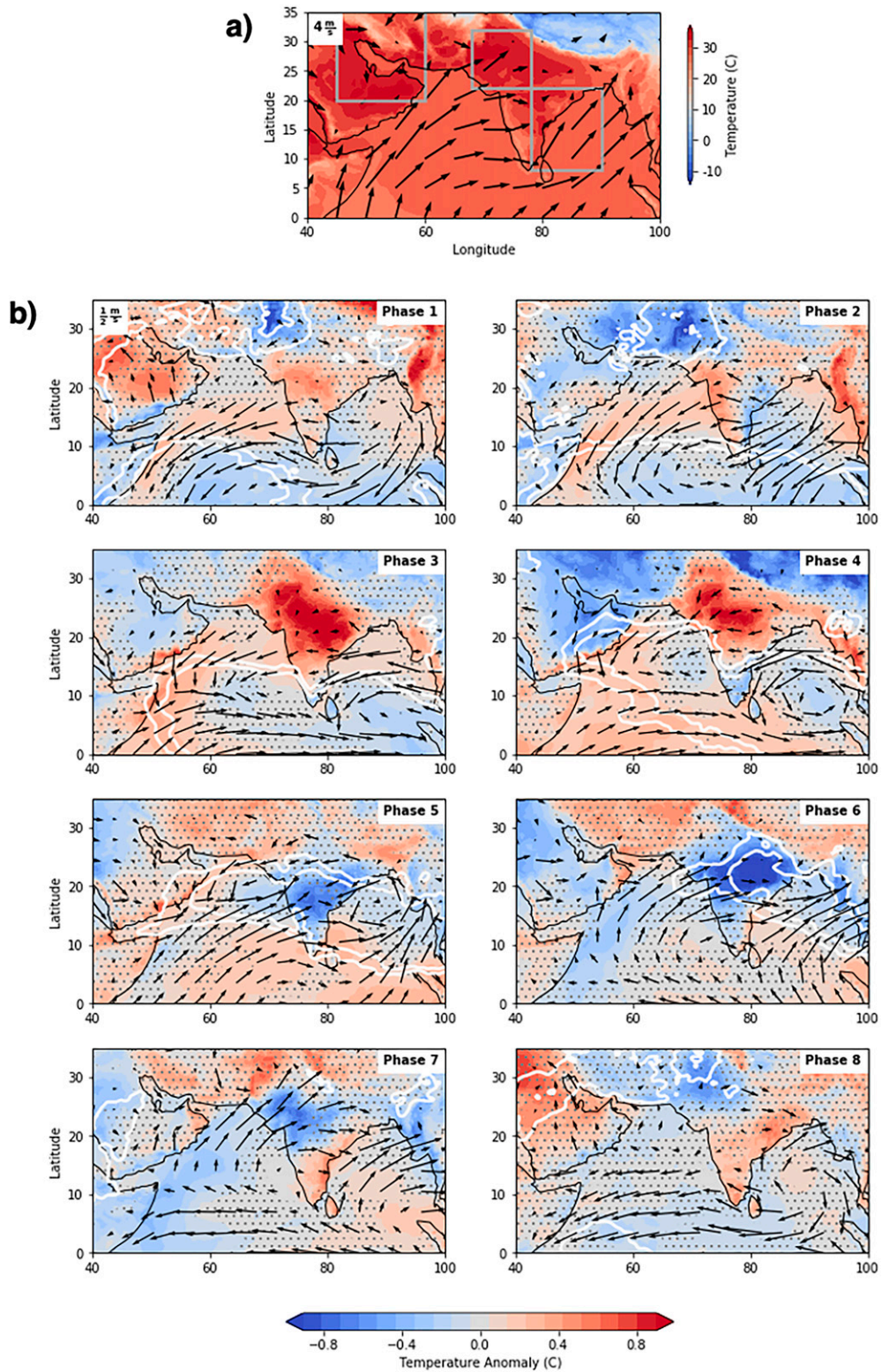


FIG. 8. ERA5 composites of daily mean 2-m air dry-bulb temperature for May–June. (a) Climatology of the region and (b) composites of daily anomalies by oscillation phase. White contours indicate location of oscillation phase. White contours indicate location of oscillation-related convection defined by OLR anomalies less than  $-4 \text{ W m}^{-2}$ , and vectors indicate surface wind anomalies. Stippling represents statistically insignificant patterns at a 95% threshold.

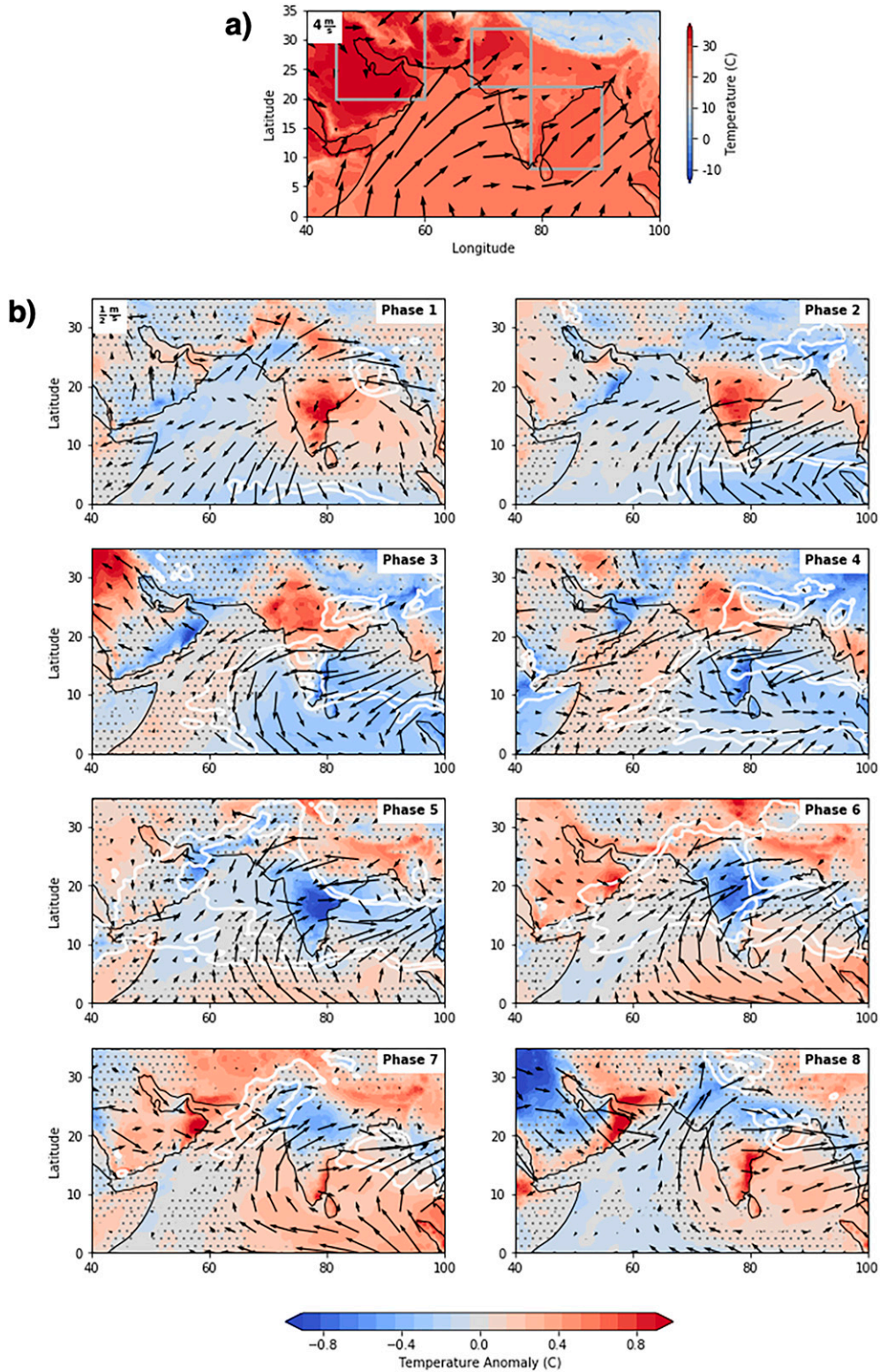


FIG. 9. ERA5 composites of daily mean 2-m air dry-bulb temperature for July–August. (a) Climatology of the region and (b) composites of daily anomalies by oscillation phase. White contours indicate location of oscillation-related convection defined by OLR anomalies less than  $-4 \text{ W m}^{-2}$ , and vectors indicate surface wind anomalies. Stippling represents statistically insignificant patterns at a 95% threshold.



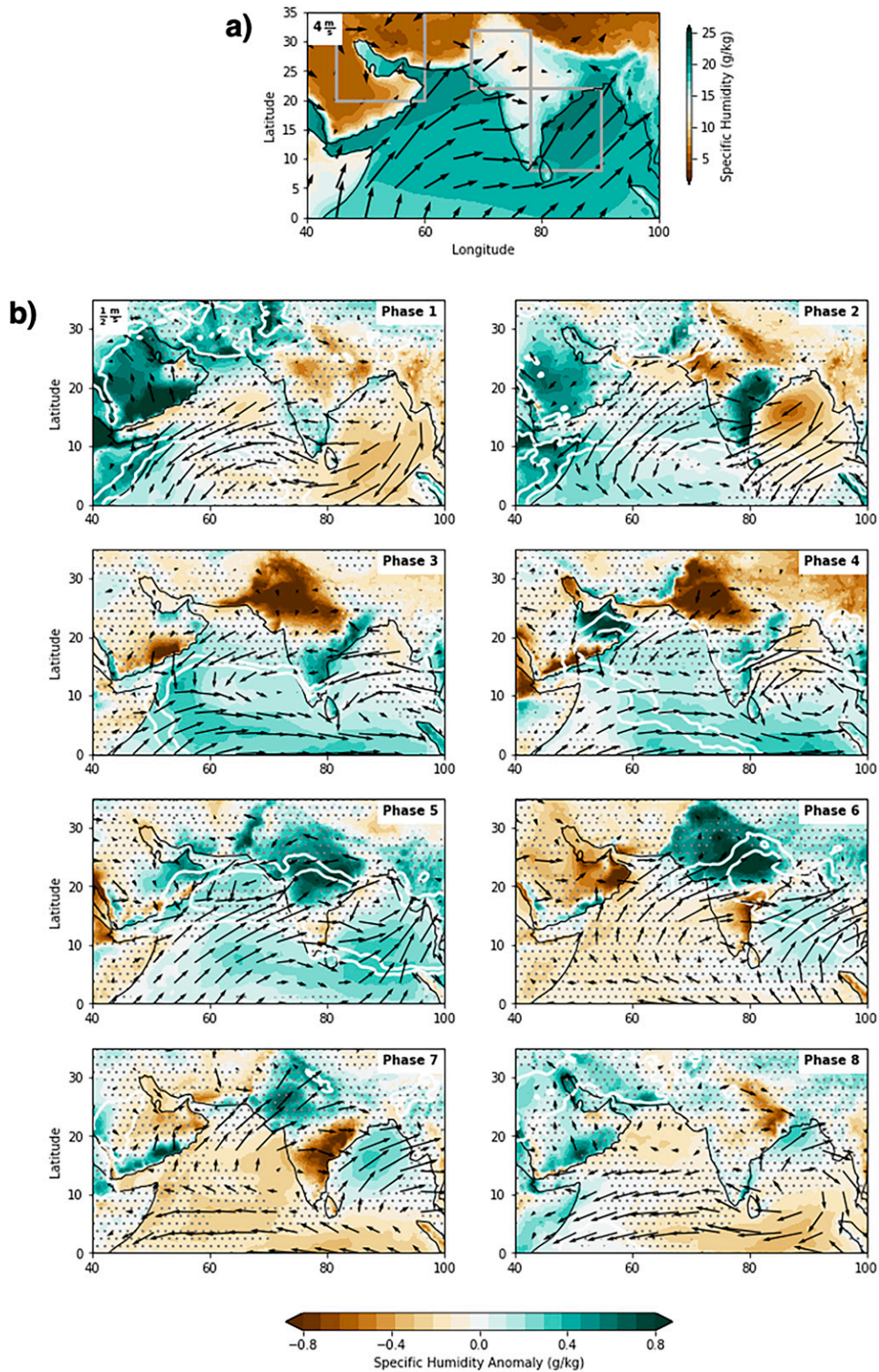


FIG. 10. ERA5 composites of daily mean 2-m specific humidity for May–June. (a) Climatology of the region and (b) composites of daily anomalies by oscillation phase. White contours indicate location of oscillation-related convection defined by OLR anomalies less than  $-4 \text{ W m}^{-2}$ , and vectors indicate surface wind anomalies. Stippling represents statistically insignificant patterns at a 95% threshold.

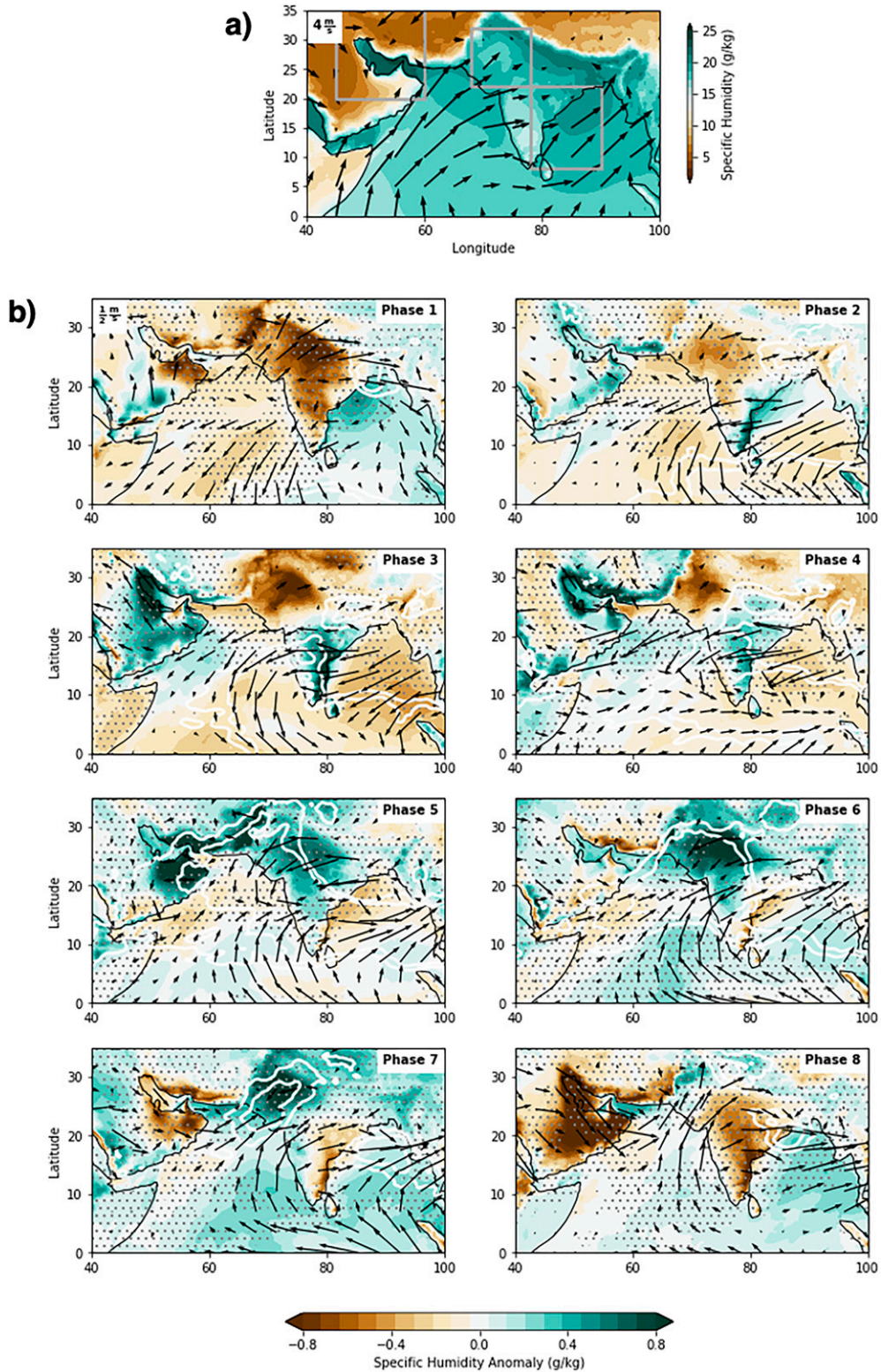


FIG. 11. ERA5 composites of daily mean 2-m specific humidity for July–August. (a) Climatology of the region and (b) composites of daily anomalies by oscillation phase. White contours indicate location of oscillation-related convection defined by OLR anomalies less than  $-4 \text{ W m}^{-2}$ , and vectors indicate surface wind anomalies. Stippling represents statistically insignificant patterns at a 95% threshold.



in the northern portion of the region, where the highest frequency of extremes occurs according to the station data (Figs. 8 and 10). There are also strong easterly surface wind anomalies, which are associated with monsoon breaks. These results are consistent with Joseph et al. (2009, 2022), who suggested that the MJO serves to initiate monsoon breaks via the northwestward propagation of a Rossby wave that acts to suppress convection in the Indian region. This tends to occur when the suppressed phase of the MJO is centered over the Indian Ocean. During phase 1, the peak extreme phase for Bhubaneswar, there are positive wet-bulb temperature anomalies centered over the east coast of India and the Bay of Bengal (Fig. 6). Located at the northernmost edge of the southeastern India subregion, Bhubaneswar likely experiences anomalous marine advection in phase 1, while by phase 3 easterly surface level wind anomalies have migrated south into the core of this subregion. Widespread negative wet-bulb anomalies are observed during phase 5 (when extreme wet-bulb temperatures are least likely in Bhubaneswar) in the reanalysis composites, associated with strong negative temperature anomalies and positive specific humidity anomalies along the eastern coast of India. It is also during phase 5 that the easterly wind anomalies identified in earlier phases of the oscillation begin to break down and reverse to strong westerly anomalies on top of the mean climatology. The humidity anomalies shift to strongly negative and the westerly wind anomalies continue to intensify throughout phases 6 and 7 in southeastern India.

#### 4. Discussion

There is a clear intraseasonal oscillation signal observed in the wet-bulb temperatures calculated from records of stations located in both the Persian Gulf and South Asia. During Northern Hemisphere summer, the average climate of the Persian Gulf is extremely hot and dry, while the cities nearest the coast can experience more humid conditions due to their proximity to warm water. These conditions render the region well-primed for extreme humid heat during a sufficient influx of anomalous humidity on a variety of different time scales. Previous literature has suggested that sea breezes can advect water vapor over land, where it mixes with warm air of continental origin and pushes wet-bulb temperatures above dangerous thresholds (Raymond et al. 2020, 2021; Pal and Eltahir 2016). The results of this analysis suggest that during phase 3 in the July–August season, southeasterly wind anomalies are able to weaken the strength of the summer shamals, which typically move dry and hot air from the desert north of the Persian Gulf, and thereby advect humid marine air directly over the western shore. This may be similar to the physical processes that trigger the seasonal weakening of the Shamals at the end of the summer months and allow for the increase in local humidity at that time (Al Senafi and Anis 2015). The weakening observed during phase 3 may allow for longer exposure of air to the moisture overlying the Persian Gulf as the surface winds pass into the coastal regions and result in the potential for extreme wet-bulb temperatures. Further, weakened surface winds may serve to reduce vertical mixing

and allow surface humidity to build. In contrast, strong negative specific humidity anomalies occur in the Persian Gulf during phase 8 as a result of anomalous northwesterly winds, rendering this region less likely on average to experience extreme humid heat and more dependent upon anomalous bursts of humidity for those extreme events that do occur. We note that the bivariate analyses presented in this paper characterizing the average relative dependence of extreme wet-bulb temperatures on phase-specific distributions of temperature and humidity are unique to the stations analyzed, selected due to their historical risk for experiencing extreme humid heat.

Extreme wet-bulb temperatures are most likely to occur in northwestern South Asia during phase 6, with high agreement between the station and reanalysis composites. During this phase, the negative OLR anomalies centered over this region indicate enhanced convection. The associated evaporative cooling and cloud shading would be expected to suppress high wet-bulb temperatures. However, high positive humidity anomalies also occur during this phase, aligning closely with the negative OLR contours. This region experiences much warmer and drier conditions on average during July–August than the rest of South Asia. Any observation of extreme humid heat thus necessarily depends more on anomalous humidity than anomalous temperature, and likely occurs when instantaneous local conditions do not exactly match the composites. Indeed, the most extreme wet-bulb temperatures were shown to occur during phase 6 in Jacobabad with slightly higher temperatures than average. This may also suggest why negative wet-bulb temperature anomalies are observed in northwestern South Asia in reanalysis composites during phase 3. Although temperatures are hotter on average in this region during phase 3, they are accompanied by strong negative humidity anomalies associated with a lack of moisture supply and convection.

Reanalysis composites for southeastern India identify phase 3 with conditions favorable for extreme wet-bulb temperatures. The easterly surface wind anomalies observed during this phase suggest that extreme wet-bulb temperatures that occur in southeastern India may be linked to monsoon breaks. Consistent with Joseph et al. (2009), our results indicate that southeastern India experiences high wet-bulb temperatures when it is the region of suppressed convection. In this section of the oscillation circulation, anomalous subsidence works to prevent the onset of deep convection in this humid environment and encourages the buildup of warm temperatures at the surface (Rajeevan et al. 2010). These phases simultaneously experience positive humidity anomalies over southeastern India that may combine with elevated temperatures to generate extreme humid heat. Additionally, it is possible that these rising temperatures could encourage increased evapotranspiration (evaporation) from local vegetation (water bodies), further increasing the specific humidity in the region and serving as a positive feedback for extreme humid heat. The potential relationship between monsoon breaks and humid heat extremes is complex, and future research should be devoted to explicitly exploring these connections.

The difference in the influence of the intraseasonal oscillations over each subregion in South Asia is highly dependent on the background climate, the clearest component of which includes seasonal variability and the influence of the monsoon system. This contingency is in contrast to the relatively consistent phase impacts identified in the Persian Gulf. These regional differences may be due in part to their individual climatologies, but also to the relative size of each area as prescribed by this study.

While the analysis presented here demonstrates the clear influence of the MJO and BSISO over extreme wet-bulb temperatures in the Persian Gulf and South Asia, further research could be devoted to understanding the various underlying mechanisms. Close evaluation of local monsoon dynamics could help elucidate the potentially distinct controls over the occurrence and timing of extreme humid heat in the premonsoon season versus during monsoon breaks of various lengths. The complex topography and land–sea contrast in South Asia motivates future comparison of the results presented here with additional reanalysis products, particularly those at higher spatial resolution, to investigate how localized the identified patterns are. Nonlinear processes may contribute to differences in phases identified by the station and reanalysis composites. For example, the potential for convection to be either inhibited or favored locally at the daily scale may not map synchronously onto time and spatial mean conditions. These challenges may also be explored using higher-resolution reanalysis datasets. Considerations of the effect of lagged northward propagating teleconnections are beyond the scope of this work, but they could also be explored in more detail in future analyses. Motivated by the different types of humidity- and temperature-dependent humid heat extremes identified in the Persian Gulf and South Asia, evaluating how human health or other societal systems are affected by these different types of humid heat extremes could be beneficial to scientific, policy, and practitioner communities when considering local impacts.

## 5. Conclusions

This analysis explores the influence of the Madden–Julian oscillation and boreal summer intraseasonal oscillation on the subseasonal-to-seasonal variability of wet-bulb temperature in two regions that already experience briefly intolerable levels of humid heat. We find that extreme wet-bulb temperatures are more than twice as likely in some oscillation phases as in others in both the Persian Gulf and South Asia during the May–June and July–August seasons. In the Persian Gulf throughout July–August, during phase 3 southeasterly surface wind anomalies weaken the northwesterly summer shamal winds and allow higher humidity anomalies to build up in the coastal regions of the Persian Gulf, perhaps due both to the increased time spent by air masses over the warm gulf before reaching the coastal land and to reduced vertical mixing associated with the weaker surface winds. In an already extremely hot and arid climate, this allows for the exceedance of extreme wet-bulb temperatures in this region. Future research

could explore these mechanisms in more detail, and for individual events.

Two different mechanisms appear to control the influence of the MJO and BSISO on extreme humid heat in the analyzed subregions of South Asia, operating on top of the unique regional background climatologies. On the eastern coast of India, easterly wind anomalies associated with phase 3 indicate that extreme summer wet-bulb temperatures in this region may take place during monsoon breaks. Monsoon onset in South Asia progresses from south to north, typically beginning close to the end of May at the southernmost tip of India (Qian and Lee 1999). The increased cloud shading and evaporative cooling taking place during this season due to strong and frequent precipitation renders summer relatively cool in comparison to the premonsoon season. Suppressed convection associated with oscillation-related circulation may encourage sustained monsoon breaks, during which time surface air temperatures can increase and allow for extreme humid heat to occur. In contrast, in Pakistan and northwestern India, monsoon onset occurs in early to mid-July, and the climate is warmer and drier. The highest wet-bulb temperatures that occur in this subregion take place during or just ahead of the arrival of the center of enhanced convection, increasing specific humidity within the region.

The implications of humid heat extend beyond human health outcomes. At moderate levels of humid heat, negative economic impacts can be incurred through decreased labor productivity (Zander et al. 2015; Borg et al. 2021). Further, greatly increased energy demand can be expected to accompany the projected rise in extreme humid heat due to the need for artificial cooling (Davis and Gertler 2015). Understanding the subseasonal-to-seasonal variability of humid heat is particularly important, as this time scale represents a prediction gap between weather and climate. Many obstacles still remain in predicting the onset and propagation of the MJO and BSISO (Jiang et al. 2020). However, recent literature has suggested that the oscillations may be predictable out to four weeks (Vitart 2017), enhancing the prospect of improving our understanding of when extreme humid heat may occur. Investigating the drivers of extreme wet-bulb temperatures can help the public health sector, energy providers, and government officials to develop and execute humid heat resilience plans. Improving our understanding of the short- and long-term influences of extreme wet-bulb temperatures thus has the potential to reduce the manifold health and economic impacts of humid heat.

*Acknowledgments.* Funding for C. Ivanovich and R. Horton was provided by National Oceanic and Atmospheric Administration's Regional Integrated Sciences and Assessments program, Grant NA15OAR4310147. C. Raymond's portion of the work was carried out at the Jet Propulsion Laboratory, California Institute of Technology, under a contract with the National Aeronautics and Space Administration (80NM0018D0004). A. H. Sobel acknowledges support from NSF Grant AGS-1758603. The authors declare no conflicts of interest with regard to this research.

*Data availability statement.* All datasets used in this analysis are publicly accessible via the following websites: HadISD, <https://www.metoffice.gov.uk/hadobs/hadisd/>; and ERA5, <https://www.ecmwf.int/en/forecasts/datasets/reanalysis-datasets/era5>.

## REFERENCES

- Acosta, R. P., and M. Huber, 2017: The neglected Indo-Gangetic Plains low-level jet and its importance for moisture transport and precipitation during the peak summer monsoon. *Geophys. Res. Lett.*, **44**, 8601–8610, <https://doi.org/10.1002/2017GL074440>.
- Adames, A. F., J. M. Wallace, and J. M. Monteiro, 2016: Seasonality of the structure and propagation characteristics of the MJO. *J. Atmos. Sci.*, **73**, 3511–3526, <https://doi.org/10.1175/JAS-D-15-0232.1>.
- Al Senafi, F., and A. Anis, 2015: Shamals and climate variability in the northern Arabian/Persian Gulf from 1973 to 2012. *Int. J. Climatol.*, **35**, 4509–4528, <https://doi.org/10.1002/joc.4302>.
- Alvarez, M. S., C. S. Vera, G. N. Kiladis, and B. Liebmann, 2016: Influence of the Madden–Julian oscillation on precipitation and surface air temperature in South America. *Climate Dyn.*, **46**, 245–262, <https://doi.org/10.1007/s00382-015-2581-6>.
- Arcodia, M. C., B. P. Kirtman, and L. S. P. Siqueira, 2020: How MJO teleconnections and ENSO interference impacts U.S. precipitation. *J. Climate*, **33**, 4621–4640, <https://doi.org/10.1175/JCLI-D-19-0448.1>.
- Barlow, M., M. Wheeler, B. Lyon, and H. Cullen, 2005: Modulation of daily precipitation over southwest Asia by the Madden–Julian oscillation. *Mon. Wea. Rev.*, **133**, 3579–3594, <https://doi.org/10.1175/MWR3026.1>.
- Bohren, C. F., and B. A. Albrecht, 1998: *Atmospheric Thermodynamics*. Oxford University Press, 417 pp.
- Borg, M. A., and Coauthors, 2021: Occupational heat stress and economic burden: A review of global evidence. *Environ. Res.*, **195**, 110781, <https://doi.org/10.1016/j.envres.2021.110781>.
- Buzan, J. R., and M. Huber, 2020: Moist heat stress on a hotter Earth. *Annu. Rev. Earth Planet. Sci.*, **48**, 623–655, <https://doi.org/10.1146/annurev-earth-053018-060100>.
- , K. Oleson, and M. Huber, 2015: Implementation and comparison of a suite of heat stress metrics within Community Land Model version 4.5. *Geosci. Model Dev.*, **8**, 151–170, <https://doi.org/10.5194/gmd-8-151-2015>.
- Cheng, Y., S. C. Lung, and J. Hwang, 2019: New approach to identifying proper thresholds for a heat warning system using health risk increments. *Environ. Res.*, **170**, 282–292, <https://doi.org/10.1016/j.envres.2018.12.059>.
- Coffel, E. D., R. M. Horton, and A. de Sherbinin, 2018: Temperature and humidity based projections of a rapid rise in global heat stress exposure during the 21st century. *Environ. Res. Lett.*, **13**, 014001, <https://doi.org/10.1088/1748-9326/aaa00e>.
- Coughlan de Perez, E., and Coauthors, 2018: Global predictability of temperature extremes. *Environ. Res. Lett.*, **13**, 054017, <https://doi.org/10.1088/1748-9326/aab94a>.
- Davies-Jones, R., 2008: An efficient and accurate method for computing the wet-bulb temperature along pseudoadiabats. *Mon. Wea. Rev.*, **136**, 2764–2785, <https://doi.org/10.1175/2007MWR2224.1>.
- Davis, L. W., and P. J. Gertler, 2015: Contribution of air conditioning adoption to future energy use under global warming. *Proc. Natl. Acad. Sci. USA*, **112**, 5962–5967, <https://doi.org/10.1073/pnas.1423558112>.
- Di Napoli, C., F. Pappenberger, and H. L. Cloke, 2019: Verification of heat stress thresholds for a health-based heat-wave definition. *J. Appl. Meteor. Climatol.*, **58**, 1177–1194, <https://doi.org/10.1175/JAMC-D-18-0246.1>.
- Dunn, R. J. H., 2019: HadISD version 3: Monthly updates. Met Office Hadley Centre Tech. Note 103, 10 pp.
- Feng, M., and Coauthors, 2020: Tracking air–sea exchange and upper-ocean variability in the Indonesian–Australian basin during the onset of the 2018/19 Australian summer monsoon. *Bull. Amer. Meteor. Soc.*, **101**, E1397–E1412, <https://doi.org/10.1175/BAMS-D-19-0278.1>.
- Gagnon, D., and C. G. Crandall, 2018: Sweating as a heat loss thermoeffector. *Handbook of Clinical Neurology*, Vol. 156, Elsevier, 211–232, <https://doi.org/10.1016/B978-0-444-63912-7.00013-8>.
- Hersbach, H., and Coauthors, 2020: The ERA5 global reanalysis. *Quart. J. Roy. Meteor. Soc.*, **146**, 1999–2049, <https://doi.org/10.1002/qj.3803>.
- Horton, R. M., J. S. Mankin, C. Lesk, E. Coffel, and C. Raymond, 2016: A review of recent advances in research on extreme heat events. *Curr. Climate Change Rep.*, **2**, 242–259, <https://doi.org/10.1007/s40641-016-0042-x>.
- Im, E. S., M. P. Marcella, and E. A. B. Eltahir, 2014: Impact of potential large-scale irrigation on the West African monsoon and its dependence on location of irrigated area. *J. Climate*, **27**, 994–1009, <https://doi.org/10.1175/JCLI-D-13-00290.1>.
- , J. S. Pal, and E. A. B. Eltahir, 2017: Deadly heat waves projected in the densely populated agricultural regions of South Asia. *Sci. Adv.*, **3**, e1603322, <https://doi.org/10.1126/sciadv.1603322>.
- Jeong, J., C. Ho, B. Kim, and W. Kwon, 2005: Influence of the Madden–Julian oscillation on wintertime surface air temperature and cold surges in East Asia. *J. Geophys. Res.*, **110**, D11104, <https://doi.org/10.1029/2004JD005408>.
- Jiang, X., T. Li, and B. Wang, 2004: Structures and mechanisms of the northward propagating boreal summer intraseasonal oscillation. *J. Climate*, **17**, 1022–1039, [https://doi.org/10.1175/1520-0442\(2004\)017<1022:SAMOTN>2.0.CO;2](https://doi.org/10.1175/1520-0442(2004)017<1022:SAMOTN>2.0.CO;2).
- , and Coauthors, 2020: Fifty years of research on the Madden–Julian oscillation: Recent progress, challenges, and perspectives. *J. Geophys. Res. Atmos.*, **125**, e2019JD030911, <https://doi.org/10.1029/2019JD030911>.
- Joseph, S., A. K. Sahai, and B. N. Goswami, 2009: Eastward propagating MJO during boreal summer and Indian monsoon droughts. *Climate Dyn.*, **32**, 1139–1153, <https://doi.org/10.1007/s00382-008-0412-8>.
- , —, H. Shabu, R. Chattopadhyay, and M. Kaur, 2022: Recent changes in the spatio-temporal characteristics of monsoon intraseasonal oscillations. *Theor. Appl. Climatol.*, **147**, 251–264, <https://doi.org/10.1007/s00704-021-03830-7>.
- Kiladis, G. N., J. Dias, K. H. Straub, M. C. Wheeler, S. N. Tulich, K. Kikuchi, K. M. Weickmann, and M. J. Ventrice, 2014: A comparison of OLR and circulation-based indices for tracking the MJO. *Mon. Wea. Rev.*, **142**, 1697–1715, <https://doi.org/10.1175/MWR-D-13-00301.1>.
- Kjellstrom, T., D. Briggs, C. Freyberg, B. Lemke, M. Otto, and O. Hyatt, 2016: Heat, human performance, and occupational health: A key issue for the assessment of global climate change impacts. *Annu. Rev. Public Health*, **37**, 97–112, <https://doi.org/10.1146/annurev-publhealth-032315-021740>.

- Kovats, R. S., and S. Hajat, 2008: Heat stress and public health: A critical review. *Annu. Rev. Public Health*, **29**, 41–55, <https://doi.org/10.1146/annurev.publhealth.29.020907.090843>.
- Krakauer, N. Y., B. I. Cook, and M. J. Puma, 2020: Effect of irrigation on humid heat extremes. *Environ. Res. Lett.*, **15**, 094010, <https://doi.org/10.1088/1748-9326/ab9ecf>.
- Lawrence, D. M., and P. J. Webster, 2002: The boreal summer intraseasonal oscillation: Relationship between northward and eastward movement of convection. *J. Atmos. Sci.*, **59**, 1593–1606, [https://doi.org/10.1175/1520-0469\(2002\)059<1593:TBSIOR>2.0.CO;2](https://doi.org/10.1175/1520-0469(2002)059<1593:TBSIOR>2.0.CO;2).
- Leon, L. R., and A. Bouchama, 2015: Heat stroke. *Compr. Physiol.*, **5**, 611–647, <https://doi.org/10.1002/cphy.c140017>.
- Lin, H., and G. Brunet, 2009: The influence of the Madden–Julian oscillation on Canadian wintertime surface air temperature. *Mon. Wea. Rev.*, **137**, 2250–2262, <https://doi.org/10.1175/2009MWR2831.1>.
- Lutsko, N. J., 2020: The relative contributions of temperature and moisture to heat stress changes under warming. *J. Climate*, **34**, 901–917, <https://doi.org/10.1175/JCLI-D-20-0262.1>.
- Mishra, V., A. K. Ambika, A. Asoka, S. Aadhar, J. Buzan, R. Kumar, and M. Huber, 2020: Moist heat stress extremes in India enhanced by irrigation. *Nat. Geosci.*, **13**, 722–728, <https://doi.org/10.1038/s41561-020-00650-8>.
- Monteiro, J. M., and R. Caballero, 2019: Characterization of extreme wet-bulb temperature events in southern Pakistan. *Geophys. Res. Lett.*, **46**, 10 659–10 668, <https://doi.org/10.1029/2019GL084711>.
- Mora, C., and Coauthors, 2017: Global risk of deadly heat. *Nat. Climate Change*, **7**, 501–506, <https://doi.org/10.1038/nclimate3322>.
- Nasrallah, H. A., E. Nieplova, and E. Ramadan, 2004: Warm season extreme temperature events in Kuwait. *J. Arid Environ.*, **56**, 357–371, [https://doi.org/10.1016/S0140-1963\(03\)00007-7](https://doi.org/10.1016/S0140-1963(03)00007-7).
- Pal, J. S., and E. A. B. Eltahir, 2016: Future temperature in southwest Asia projected to exceed a threshold for human adaptability. *Nat. Climate Change*, **6**, 197–200, <https://doi.org/10.1038/nclimate2833>.
- Parsons, K., 2006: Heat stress standard ISO 7243 and its global application. *Ind. Health*, **44**, 368–379, <https://doi.org/10.2486/indhealth.44.368>.
- Pradhan, B., T. Kjellstrom, D. Atar, P. Sharma, B. Kayastha, G. Bhandari, and P. K. Pradhan, 2019: Heat stress impacts on cardiac mortality in Nepali migrant workers in Qatar. *Cardiology*, **143**, 37–48, <https://doi.org/10.1159/000500853>.
- Prasanna, V., and H. Annamalai, 2012: Moist dynamics of extended monsoon breaks over South Asia. *J. Climate*, **25**, 3810–3831, <https://doi.org/10.1175/JCLI-D-11-00459.1>.
- Qian, W., and D. Lee, 1999: Seasonal march of Asian summer monsoon. *Int. J. Climatol.*, **20**, 1371–1386, [https://doi.org/10.1002/1097-0088\(200009\)20:11<1371::AID-JOC538>3.0.CO;2-V](https://doi.org/10.1002/1097-0088(200009)20:11<1371::AID-JOC538>3.0.CO;2-V).
- Rajeevan, M., S. Gadgil, and J. Bhate, 2010: Active and break spells of the Indian summer monsoon. *J. Earth Syst. Sci.*, **119**, 229–247, <https://doi.org/10.1007/s12040-010-0019-4>.
- Raymond, C., D. Singh, and R. M. Horton, 2017: Spatiotemporal patterns and synoptics of extreme wet-bulb temperature in the contiguous United States. *J. Geophys. Res. Atmos.*, **122**, 13 108–13 124, <https://doi.org/10.1002/2017JD027140>.
- , and Coauthors, 2019: Projections and hazards of future extreme heat. *The Oxford Handbook of Planning for Climate Change Hazards*, W. T. Pfeffer, J. B. Smith, and K. L. Ebi, Eds., Oxford University Press, 10.1093/oxfordhb/9780190455811.013.59.
- , T. Matthews, and R. M. Horton, 2020: The emergence of heat and humidity too severe for human tolerance. *Sci. Adv.*, **6**, eaaw1838, <https://doi.org/10.1126/sciadv.aaw1838>.
- , —, —, E. M. Fischer, C. Ivanovich, L. Suarez-Gutierrez, and Y. Zhang, 2021: On the controlling factors for globally extreme humid heat. *Geophys. Res. Lett.*, **48**, e2021gl096082, <https://doi.org/10.1029/2021GL096082>.
- Rodwell, M. J., and B. J. Hoskins, 1996: Monsoons and the dynamics of deserts. *Quart. J. Roy. Meteor. Soc.*, **122**, 1385–1404, <https://doi.org/10.1002/qj.49712253408>.
- Semenza, J. C., J. E. McCullough, W. D. Flanders, M. A. McGeehin, and J. R. Lumpkin, 1999: Excess hospital admissions during the July 1995 heat wave in Chicago. *Amer. J. Prev. Med.*, **16**, 269–277, [https://doi.org/10.1016/S0749-3797\(99\)00025-2](https://doi.org/10.1016/S0749-3797(99)00025-2).
- Sherwood, S. C., and M. Huber, 2010: An adaptability limit to climate change due to heat stress. *Proc. Natl. Acad. Sci. USA*, **107**, 9552–9555, <https://doi.org/10.1073/pnas.0913352107>.
- Sikka, D. R., and S. Gadgil, 1980: On the maximum cloud zone and the ITCZ over Indian longitudes during the southwest monsoon. *Mon. Wea. Rev.*, **108**, 1840–1853, [https://doi.org/10.1175/1520-0493\(1980\)108<1840:OTMCZA>2.0.CO;2](https://doi.org/10.1175/1520-0493(1980)108<1840:OTMCZA>2.0.CO;2).
- Stull, R., 2011: Wet-bulb temperature from relative humidity and air temperature. *J. Appl. Meteor. Climatol.*, **50**, 2267–2269, <https://doi.org/10.1175/JAMC-D-11-0143.1>.
- Vecellio, D. J., S. T. Wolf, R. M. Cottle, and W. L. Kenney, 2022: Evaluating the 35°C wet-bulb temperature adaptability threshold for young, healthy subjects (PSU HEAT Project). *J. Appl. Physiol.*, **132**, 340–345, <https://doi.org/10.1152/jappphysiol.00738.2021>.
- Vitart, F., 2017: Madden–Julian oscillation prediction and teleconnections in the S2S database. *Quart. J. Roy. Meteor. Soc.*, **143**, 2210–2220, <https://doi.org/10.1002/qj.3079>.
- Wang, B., and X. Xie, 1997: A model for the boreal summer intraseasonal oscillation. *J. Atmos. Sci.*, **54**, 72–86, [https://doi.org/10.1175/1520-0469\(1997\)054<0072:AMFTBS>2.0.CO;2](https://doi.org/10.1175/1520-0469(1997)054<0072:AMFTBS>2.0.CO;2).
- Wang, S., and A. H. Sobel, 2022: A unified moisture mode theory for the Madden–Julian oscillation and boreal summer intraseasonal oscillation. *J. Climate*, **35**, 1267–1291, <https://doi.org/10.1175/JCLI-D-21-0361.1>.
- , D. Ma, A. H. Sobel, and M. K. Tippett, 2018: Propagation characteristics of BSISO indices. *Geophys. Res. Lett.*, **45**, 9934–9943, <https://doi.org/10.1029/2018GL078321>.
- Wheeler, M. C., and H. H. Hendon, 2004: An all-season real-time multivariate MJO index: Development of an index for monitoring and prediction. *Mon. Wea. Rev.*, **132**, 1917–1932, [https://doi.org/10.1175/1520-0493\(2004\)132<1917:AARMMI>2.0.CO;2](https://doi.org/10.1175/1520-0493(2004)132<1917:AARMMI>2.0.CO;2).
- , —, S. Cleland, H. Meinke, and A. Donald, 2008: Impacts of the Madden–Julian oscillation on Australian rainfall and circulation. *J. Climate*, **22**, 1482–1498, <https://doi.org/10.1175/2008JCLI2595.1>.
- Wilks, D. S., 2016: “The stippling shows statistically significant grid points”: How research results are routinely overstated and overinterpreted, and what to do about it. *Bull. Amer. Meteor. Soc.*, **97**, 2263–2273, <https://doi.org/10.1175/BAMS-D-15-00267.1>.
- Xue, P., and E. A. B. Eltahir, 2015: Estimation of the heat and water budgets of the Persian (Arabian) Gulf using a regional climate model. *J. Climate*, **28**, 5041–5062, <https://doi.org/10.1175/JCLI-D-14-00189.1>.



- Yasunari, T., 1979: Cloudiness fluctuations associated with the Northern Hemisphere summer monsoon. *J. Meteor. Soc. Japan*, **57**, 227–242, [https://doi.org/10.2151/jmsj1965.57.3\\_227](https://doi.org/10.2151/jmsj1965.57.3_227).
- Zander, K. K., W. J. W. Botzen, E. Oppermann, and T. Kjellstrom, and S. T. Gernett, 2015: Heat stress causes substantial labour productivity loss in Australia. *Nat. Climate Change*, **5**, 647–651, <https://doi.org/10.1038/nclimate2623>.
- Zhang, C., 2005: Madden–Julian oscillation. *Rev. Geophys.*, **43**, RG2003, <https://doi.org/10.1029/2004RG000158>.
- Zhou, S., M. L'Heureux, S. Weaver, and A. Kumar, 2012: A composite study of the MJO influence on the surface air temperature and precipitation over the continental United States. *Climate Dyn.*, **38**, 1459–1471, <https://doi.org/10.1007/s00382-011-1001-9>.